CRYSTAL GROWTH & DESIGN

Article

Cite This: Cryst. Growth Des. 2017, 17, 5652-5659

pubs.acs.org/crystal

Room Temperature Magnesite Precipitation

Ian M. Power,*[,†] Paul A. Kenward,[‡] Gregory M. Dipple,[‡] and Mati Raudsepp[‡]

[†]School of the Environment, Trent University, 1600 West Bank Drive, Peterborough, Ontario K9L 0G2, Canada

[‡]Department of Earth, Ocean and Atmospheric Sciences, The University of British Columbia, 2207 Main Mall, Vancouver, British Columbia V6T 1Z4, Canada

Supporting Information

ABSTRACT: Magnesite ($MgCO_3$) is one of the most stable sinks for carbon dioxide (CO_2) and is therefore of great interest for long-term carbon storage. Although magnesite is the thermodynamically stable form of magnesium carbonate, the kinetic inhibition of low-temperature precipitation has hindered the development of carbon sequestration strategies that can be economically conducted under ambient temperature. Here, we document the precipitation of magnesite from waters (magnesite saturation index = 1.45) in batch reactors at room temperature with the aid of carboxylated polystyrene microspheres over the course of 70 days. Microspheres provide surfaces with a high density of carboxyl groups that act to bind and dehydrate Mg^{2+} ions in solution, thereby minimizing the kinetic barrier and facilitating magnesite formation. Magnesite crystals are observed on sphere surfaces and their organic matrixes. Mineral identification was confirmed by X-ray diffraction and selected area electron diffraction of a thin section obtained by focused ion beam milling. We demonstrate that kinetic barriers to magnesite formation can be overcome at ambient conditions. Incorporating surfaces with high carboxyl site densities into ex situ mineral carbonation processes and the use of such ligands for deep geologic CO_2 storage may offer novel and economically viable strategies for permanent carbon storage.

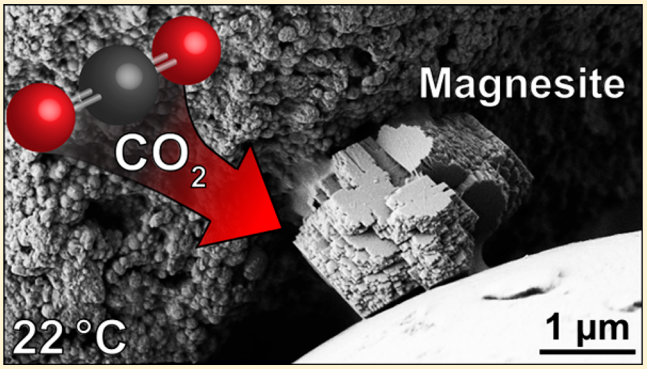

1. INTRODUCTION

Mechanisms of carbonate formation have long been studied to further our understanding of carbonate depositional environments, yet this area of research has gained greater attention because of its relevance to permanent storage of carbon dioxide (CO_2) in both ex situ mineral carbonation processes and deep geologic storage.[1−3] Ex situ mineral carbonation technologies aim to capitalize on the globally abundant natural deposits of ultramafic and mafic rocks by forming magnesite ($MgCO_3$) as a stable sink for CO_2.[1] These proposed technologies are usually operated at high temperature and pressure to achieve fast carbonation rates; however, these approaches are not yet economically viable with current technology.[3] At low temperatures, carbonation of Mg-bearing feedstock, either abiotically or biologically, results in the precipitation of metastable hydrated Mg-carbonate minerals such as nesquehonite ($MgCO_3·3H_2O$), dypingite [$Mg_5(CO_3)_4(OH)_2·5H_2O$], and hydromagnesite [$Mg_5(CO_3)_4(OH)_2·4H_2O$].[4−9] These metastable phases require considerably more onerous chemical conditions (e.g., higher Mg concentration) than those required to reach magnesite saturation.[10] This conundrum in balancing carbonation rates with acceptable costs has spurred a wealth of scientific inquiry with the goal of developing economically feasible carbonation pathways.

Magnesite and dolomite [$CaMg(CO_3)_2$] have precipitation rates that are orders of magnitude slower than calcite ($CaCO_3$) at Earth's surface conditions, which has hampered the formation of these minerals in the laboratory at room temperature.[9,11−13] These sluggish rates have hindered our understanding of magnesite formation in natural environments and have generally restricted carbon sequestration technologies that form magnesite to high temperature systems.[3,11] However, magnesite has successfully been precipitated at 35 °C using supercritical CO_2.[14−17] At ambient pressure and low temperatures (<60 °C), magnesite precipitation is kinetically inhibited due to the strong hydration of magnesium (Mg^{2+}) ions in solution.[10,18] This is the same root cause behind the *dolomite problem*, which is defined by the disparity between the abundance of dolomite in the geologic record and its paucity in modern environments despite being supersaturated in seawater. The "problem" is one of kinetics, and given sufficient time, precipitation rates are adequate to explain the occurrence of dolomite as well as magnesite in the geologic record without mediation or acceleration.[19]

Several studies have succeeded in increasing rates of disordered or ordered dolomite precipitation at low temperature to observe its formation at the laboratory time scale and to begin to demystify the processes that may accelerate its

Received: March 2, 2017
Revised: June 28, 2017
Published: October 6, 2017

DOI: 10.1021/acs.cgd.7b00311
Cryst. Growth Des. 2017, 17, 5652−5659

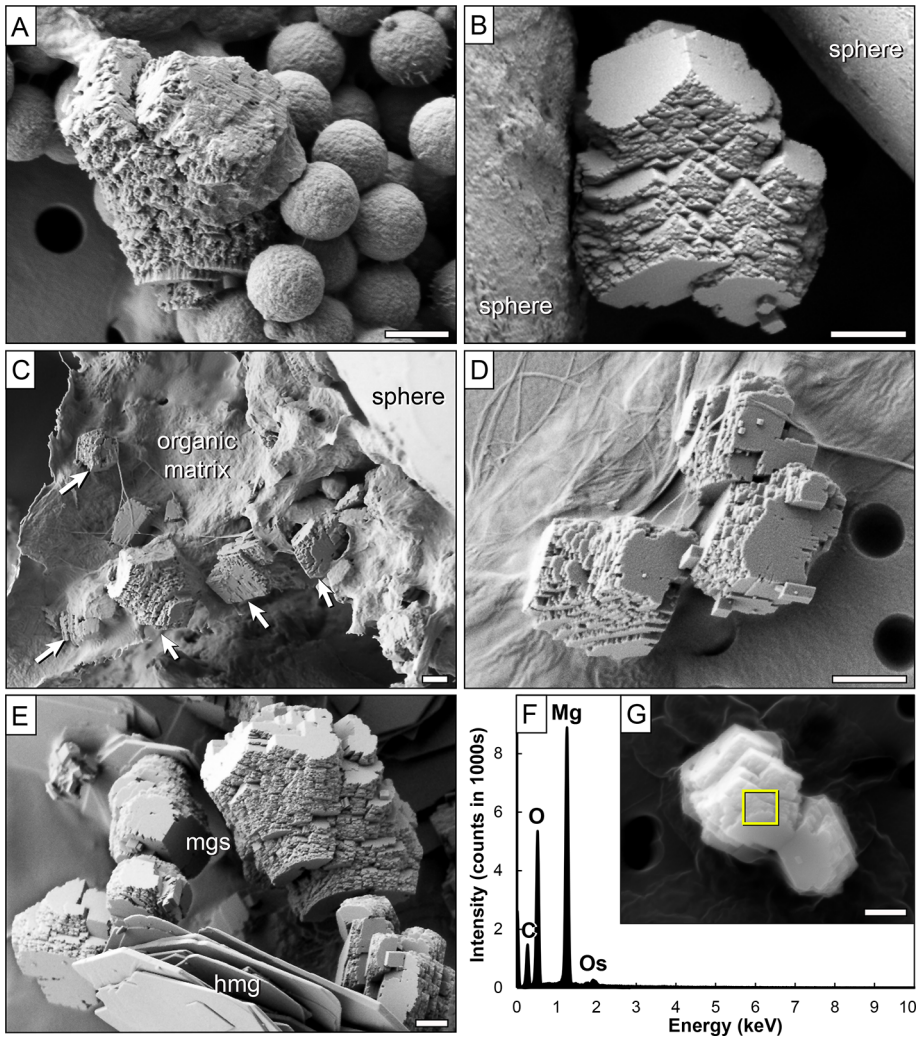

Figure 1. Representative scanning electron micrographs of polystyrene microspheres and associated mineral precipitates after 60 days of reaction. (A) Low carboxyl site density spheres with unidentified mineral precipitate. (B) Mineral precipitate on high carboxyl site density sphere showing step growth texture. (C) Numerous mineral precipitates (arrows) held in an organic matrix attached to a sphere (upper right). (D) Mineral precipitates on filter paper exhibiting attachment and aggregation. (E) For comparison, naturally occurring magnesite from a hydromagnesite-magnesite playa. (F) Representative energy dispersive spectrum of mineral precipitate (G) revealing the chemical composition of Mg, C, and O (Os is from coating). Scale bars are 500 nm.

formation in sedimentary environments.[20−23] The dehydration of Mg^{2+} ions is considered the rate-limiting step for the precipitation of both dolomite and magnesite at low temperature.[11] Kenward et al.[21] demonstrated that carboxyl functional groups on microbial cell walls could bind and partially dehydrate Mg^{2+} ions in an energetically favorable process that facilitates dolomite precipitation. This mechanism was validated with the use of densely carboxylated microspheres to abiotically precipitate dolomite from solution at 30 °C.[22] In the present study, we show the formation of magnesite at room temperature with the aid of carboxylated polystyrene microspheres in solutions slightly supersaturated with respect to magnesite. Manipulation of this reaction pathway to accelerate magnesite formation at low temperature may provide an economical alternative for carbon storage, as there likely would be substantially less energy required in comparison to high temperature and pressure systems.

2. EXPERIMENTAL SECTION

2.1. Batch Experiments. Batch reactors were used to examine the precipitation of magnesite at room temperature (~22 °C). Experimental solutions (100 mL of deionized water) were composed of 10 mM $NaHCO_3$ and 10 mM $MgCl_2{\cdot}6H_2O$ with an initial starting pH measured at 8.2. The solution chemistry had a magnesite saturation index (SI) of 1.45 as calculated using PHREEQC V.3[24] with the LLNL database. Solutions were undersaturated with respect to hydromagnesite (SI = −1.91), nesquehonite (SI = −1.57), and artinite [$Mg_2(CO_3)(OH)_2{\cdot}3(H_2O)$; SI = -1.91]. Solutions were filtered (0.22 μm) and dispensed into serum vials that were sealed using butyl rubber stoppers and Al-crimp seals to prevent degassing and evaporation. Low (0.7 $COO^-/Å^2$; 0.82 μm diameter) and high (10 $COO^-/Å^2$; 20.3 μm diameter) carboxyl site density polystyrene microspheres were purchased from Bangs Laboratories Inc. These spheres were composed of 99.90% polystyrene and ≤0.10% sodium dodecyl sulfate. Reactors were amended with approximately 10^5 spheres/mL, and experiments were run in triplicate over five time intervals for each experimental condition. Reactors were not continuously mixed, and therefore, most microspheres settled to the bottom. Analyses of solutions prior to and after microsphere addition as well as after experiments showed that bulk water chemistry (pH and

DOI: 10.1021/acs.cgd.7b00311
Cryst. Growth Des. 2017, 17, 5652−5659

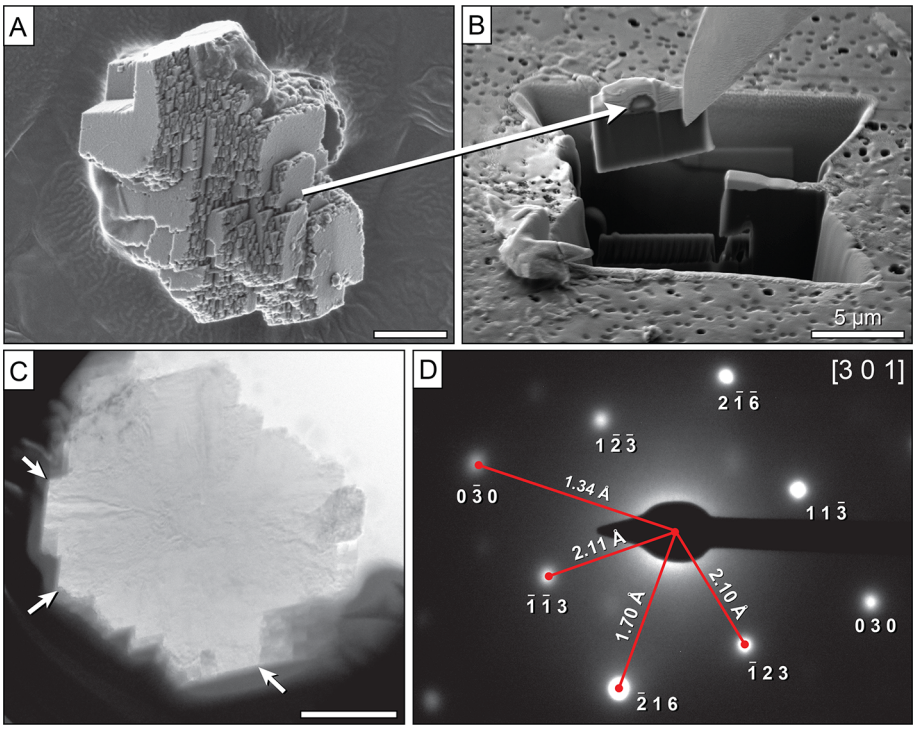

Figure 2. Electron micrographs and SAED pattern of experimental precipitate. (A) Mineral precipitate that was thin sectioned using FIB milling (B). (C) Representative transmission electron micrograph of a thin section (~100 nm thickness) of a mineral grain obtained by FIB milling. Note the outlines of rhombohedron, characteristic of magnesite (arrows). (D) An SAED pattern obtained from the mineral grain section viewing down the [3 0 1] plane. Reflections (*h k l*) are labeled with the measured lattice spacings that closely match those of magnesite (Table 1). Scale bars are 500 nm when not labeled.

[Mg]) was the same within measurement error. Reactor vessels were opened and sampled in succession, starting at 24 days of reaction with additional reactors being sampled every 12 days for a total of 72 days. Control systems either contained no microspheres or contained microspheres in deionized water. Millipore Swinnex filter holders (25 mm) and Isopore membrane filters (0.2 or 0.4 μm) were used to collect spheres and any precipitates. While remaining in filter holders, solids were rinsed using filtered deionized water to prevent formation of evaporite minerals. These solids were then dried at room temperature prior to imaging and analyses, which were done within 2 days.

2.2. Aqueous Chemistry. A portable Thermo Scientific Orion 4-Star pH/ISE probe was calibrated and used to measure the pH of experimental solutions before and after microsphere addition. The total aqueous Mg concentration of solutions was determined using inductively coupled plasma optical emission spectrometry (ICP-OES) employing a Varian 725-ES Optical Emission Spectrometer, with a detection limit of 0.2 mg/L. Reproducibility was better than 5 mg/L based on repeated analysis of standards and duplicate samples. Cation samples were acidified to 2% ultrapure HNO_3 immediately after sampling.

2.3. Scanning Electron Microscopy. Samples were imaged at the Centre for High-Throughput Phenogenomics at The University of British Columbia and Nanofabrication Facility at The University of Western Ontario. Spheres and precipitates were immobilized onto EMD Millipore Isopore membrane filters (0.2 or 0.4 μm) and flushed with deionized-distilled water to prevent evaporite minerals from forming. Filters were air-dried before mounting onto aluminum stubs using 12 mm carbon adhesive tabs. Samples were coated with either 8 nm of iridium using a Leica EM MED020 coating system or a 3 nm layer of osmium metal using a Filgen osmium plasma coater (OPC 80T). A LEO (Zeiss) 1540 XB field emission scanning electron microscope (SEM) was used to produce high-resolution images at an operating voltage of 1.0 kV. Operating the SEM at a voltage of 10 kV, an Oxford Instruments' INCAx-sight energy dispersive spectrophotometer (EDS) was utilized for elemental analysis. Focused ion beam (FIB) milling was used to obtain a thin section (~100 nm thickness) of the mineral precipitate. At the University of British Columbia, samples were imaged using an FEI Helios NanoLab 650 operating at 1.0 kV voltage.

2.4. X-ray Diffraction. Mineral phases from experiments were identified using X-ray diffraction (XRD) data. Samples were mounted as slurries onto zero diffraction quartz plates with anhydrous ethanol and allowed to dry at room temperature. All XRD data were collected using a Bruker D8 Focus Bragg–Brentano diffractometer with Co Kα radiation and a step size of 0.02° over a range of 30–70° 2θ at 2.0 s/step. A Fe monochromator foil, a 0.6 mm divergence slit, incident and diffracted beam Soller slits, and a LynxEye detector were used to collect patterns. A long, fine-focus Co X-ray tube was operated at 35 kV and 40 mA using a takeoff angle of 6°. Search-match software, DIFFRACplus EVA 14,[25] and the International Centre for Diffraction Database PDF-4+ 2010 were used for phase identification.

2.5. Transmission Electron Microscopy. Imaging of the thin section was performed at The University of British Columbia's Bioimaging Facility. The FEI Tecnai G2 transmission electron microscope (TEM) was operated at 200 kV with a LaB6 filament capable of 1.4 Å resolution. The Tecnai TEM was equipped with a high-tilt, high precision motorized stage and a high-speed AMT 2K side mount CCD camera, and a high-resolution FEI Eagle 4K bottom mount CCD camera for capturing digital images. Crystal orientation and reflections shown in the selected area electron diffraction (SAED) pattern were identified using CrystalMaker v2.7 and SingleCrystal v2.2. An electron diffraction pattern of an aluminum standard from Ted Pella Inc. (Prod. No. 619) was used to calculate lattice spacings for an unknown mineral precipitate within a FIB thin section (Table S1).

3. RESULTS AND DISCUSSION

Experiments using low carboxyl site density microspheres yielded few mineral precipitates, none of which distinctly resembled magnesite (Figure 1A). The precipitate in Figure 1A

DOI: 10.1021/acs.cgd.7b00311
Cryst. Growth Des. 2017, 17, 5652–5659

did contain Mg, C, and O based on EDS analysis. Likewise, no mineral precipitates were identified in the control experiments that lacked spheres or which contained spheres in deionized water (see the Supporting Information Figure S1A). Conversely, after 60 days of reaction, numerous (<3 μm) mineral precipitates were observed in two of the three replicate experiments that used the high carboxyl site density spheres. Precipitates appeared to be well crystalline and had rhombohedral crystal morphologies. Crystal sizes typically ranged from 200 nm to 2 μm and were in close association with microspheres and their organic matrixes (Figure 1B–D; see Figure S1 for additional micrographs). Precipitates had portions that were rhombohedral in shape, yet also had rough steplike features, indicative of spiral crystal growth.[11] Figure 1C shows numerous grains of various sizes held within an organic matrix (presumably made of styrene) hanging from a sphere. Mineral precipitates near, but not in direct contact with, spheres may have been detached during sampling (Figure 1D). Precipitates on filter paper (Figure 1D) were almost always associated with organic matrixes similar to those attached to spheres (Figure 1C). Importantly, the mineral precipitates had a markedly similar appearance to magnesite grains that have formed in the temperature range of 1–11 °C within modern hydromagnesite-magnesite playas (Figure 1E).[26,27] Very similar magnesite crystal morphologies have been noted by others in high temperature experiments.[18,28,29] Hydrated Mg-carbonate minerals such as lansfordite ($MgCO_3 \cdot 5H_2O$; short, prismatic), nesquehonite (elongated, prismatic), dypingite (rosettes, flaky), hydromagnesite (rosettes, platy), and artinite (acicular) have very different crystals morphologies than the rhombohedral crystals of magnesite.[26,30−34] Thus, the crystal morphologies of the experimental precipitates (Figure 1) are strongly indicative of magnesite.

Elemental analyses using EDS revealed that the precipitated crystals contained Mg, C, and O. This semiquantitative technique measured an average Mg:C molar ratio of 0.8:1 (n = 22), which is similar to magnesite (Figure 1F,G). Of the hydrated Mg-carbonate minerals, only lansfordite and nesquehonite have a 1:1 Mg:C molar ratio, whereas dypingite and hydromagnesite have a ratio of 5:4 and artinite has a much greater ratio of 2:1. The elemental composition and Mg:C molar ratio further support that the precipitated crystals are magnesite.

On the basis of SEM observations, the polystyrene spheres appeared to compose nearly 100% of the total solids collected. Detection limits for magnesium carbonate minerals by XRD are typically greater than ∼0.5 wt %.[35] Thus, conventional XRD analysis was hampered by the minuscule abundance of mineral precipitates and obstruction by the X-ray amorphous microspheres. Only samples from experiments with the most abundant mineral precipitates produced XRD diffraction patterns with identifiable peaks (Figure S2). XRD patterns of solids from this experiment after 60 days only showed the most intense diffraction peak for magnesite (1 0 4; d = 2.746 Å). The second (45% intensity) and third (35% intensity) most intense peaks at 50.3° and 63.5° 2θ may be hidden behind the signal from the amorphous polystyrene spheres.

A thin section was obtained using FIB milling (Figure 2A,B) and imaged using TEM (Figure 2C) with SAED patterns being collected (Figure 2D and Figure S3) to obtain a better mineral identification. Lattice spacings were calculated using an electron diffraction pattern of an aluminum standard (Figure S3A) collected under the same conditions as the pattern of the unknown mineral. The formula, $K = Sd$, was used to calculate a constant (K) that incorporates beam wavelength, camera length, and associated variable crystallographic data. S values are ring diameters (cm) of the diffraction pattern of the aluminum standard, and d is the lattice spacing in Å. An average K value for the first five rings was used to calculate the lattice spacings of the unknown precipitate. In the [3 0 1] direction, there were reflections from the 1 2 3, 1 1 3, 2 1 6, and 0 3 0 planes with measured lattice spacings of 2.10, 2.11, 1.70, and 2.34 Å, respectively. Importantly, the measurement of these lattice spacings was done independently from their identification using the software. These lattice spacings very closely match the known lattice spacing of the aforementioned planes for magnesite (Table 1). The electron diffraction data, crystal morphology, and chemical composition confirmed the precipitate to be magnesite.

Table 1. List of Reflections and Their Associated Lattice Spacings for Magnesite As Compared to Those Measured for the Unknown Mineral Precipitate (Figure 2)

reflection h k l	magnesite lattice spacing (Å)	measured lattice spacing (Å)
1 2 3	2.1022	2.10
1 1 3	2.1022	2.11
2 1 6	1.6999	1.70
0 3 0	1.3374	1.34

3.1. Precipitation Mechanisms. To our knowledge, we are the first to demonstrate the formation of magnesite, either by direct precipitation from solution or by transformation from a precursor, at room temperature. This outcome was achieved by utilizing surfaces dense in carboxyl groups to overcome the kinetic barrier associated with hydration of Mg^{2+} ions and thus accelerating magnesite precipitation. No other precipitates were detected or observed prior to identification of magnesite after 60 days of reaction. At this point, there were no signs of intergrowth between magnesite and a hydrated Mg-carbonate mineral, such as hydromagnesite, that would suggest formation from a precursor.[36] As such, direct precipitation from solution is the likely pathway for magnesite formation in this study.

Carbonate precipitation rates are related to the exchange rate of water molecules in the metal coordination hydration shell, which is 5 orders of magnitude faster for Ca^{2+} ions than the smaller, electron dense Mg^{2+} ions.[12,37] Magnesium ions have a high charge density and stable hydration spheres; the inner sphere being comprised of six water molecules in octahedral coordination.[38,39] The outer sphere is formed from 12 water molecules hydrogen-bonded to the inner sphere.[40] The net charge of a hydrated magnesium ion is $\sim 1.2^+$, indicating significant charge transfer to the surrounding water molecules.[41] The energy cost for removal of a water molecule from the outer and inner hydration spheres has been measured to be 5–12 and 20–80 kcal/mol, respectively.[38] The sluggish exchange of water molecules of $[Mg(H_2O)_6]^{2+}$ results in precipitation rates of magnesite and dolomite being 6 and 4 orders of magnitude slower than that of calcite at 25 °C, respectively.[11,12]

The inner sphere binding of $[Mg(H_2O)_6]^{2+}$ to a ligand may occur when the free energy of the substitution reaction is negative.[42] For example, the exchange of water for formate ions ($HCOO^-$), the simplest of carboxyl group compounds, is thermodynamically favorable for the first three substitutions, yet unfavorable for a fourth substitution.[42] Thus, ligands act to

DOI: 10.1021/acs.cgd.7b00311
Cryst. Growth Des. 2017, 17, 5652−5659

disrupt the inner hydration shell and remove water molecules from Mg^{2+}. Ligands can also affect the composition of carbonate minerals by preferentially binding a competing cation. For instance, carboxylated organic acids can increase the magnesium content of amorphous calcium carbonate, a calcite precursor, due to their stronger affinity for Ca^{2+} in comparison to Mg^{2+}.[43]

Microbial cell walls are host to a variety of functional groups, including carboxyl and hydroxyl groups, giving these surfaces a net negative charge.[44] Partly for this reason, microbes are thought to play an important role in precipitating dolomite and its precursors in the natural environment[20,21] and could similarly influence magnesite precipitation. Regarding low-temperature dolomite precipitation, Roberts et al.[22] emphasize the importance of surfaces with high carboxyl site densities. Nonmetabolizing archaea, *Haloferax sulfurifontis*, with a carboxyl site density of 0.1 $COO^-/Å^2$ were able to induce precipitation of dolomite.[21] As an example of organo-mineralization, Zhang et al.[23] synthesized disordered dolomite at room temperature from solutions containing either carboxymethyl cellulose or agar. Microbes and organic matter are ubiquitous to carbonate-forming environments and may provide carboxylated surfaces for dehydrating Mg^{2+} ions in nature.[21,45] For instance, there is evidence of a microbial role in magnesite formation in ancient lacustrine hypersaline environments;[46] however, clearly the conditions for low-temperature magnesite precipitation are rare given the scarcity of modern deposits.[26]

The polystyrene microspheres used by Roberts et al.[22] and in this study have a carboxyl site density that is far greater than that of an average bacterium (0.06 $COO^-/Å^2$) found in nature and *H. sulfurifontis* that was used to induce dolomite precipitation.[22] Greater carboxyl site density may partly explain the success of the high carboxyl site density spheres (10 $COO^-/Å^2$) and failure of the low carboxyl site density spheres (0.7 $COO^-/Å^2$) for precipitating magnesite. In addition to site density, the competitiveness of a ligand is also likely to affect carbonate precipitation rates and mineralogy of precipitates. Ligand competitiveness is partly determined by its charge, electron density distribution, polarizability, size, and rigidity relative to water that is binding to the cation.[42] Carboxylates have been shown to affect the relative abundances of nesquehonite and magnesite formed through the reaction of forsterite with supercritical CO_2 ($scCO_2$) at 50 °C and 90 bar.[47] Divalent carboxylates, including malonate $[CH_2(COO)_2^{2-}]$ and oxalate $[(COO)_2^{2-}]$, can form bidentate complexes that may better disrupt the inner hydration shell relative to monovalent anions, such as acetate (CH_3COO^-), that forms monodentate complexes. Trivalent citrate $[C_3H_5O(COO)_3^{3-}]$ was most effective at dehydrating Mg^{2+} ions, possibly due in part to the affinity of its hydroxyl group for cations.[47] Polycarboxylates may be more effective in dehydrating Mg^{2+} ions in a similar fashion as having a surface with a high carboxyl site density.

Molecular dynamics simulations investigating the effect of $Mg-H_2O$ interaction on dolomite crystal growth revealed that Mg is thermodynamically easily incorporated into a calcite crystal, but then inhibits incorporation of Ca unless water is removed from the surface.[48] Consequently, a reduction in water activity may aid in incorporating magnesium ions. For instance, Xu et al.[49] were able to form amorphous magnesium carbonate and increase magnesium substitution into calcite precipitated in formamide, a nonaqueous solvent. In our experiments, magnesite crystals were commonly observed with an organic matrix (e.g., Figure 1C), the volume of which was likely reduced under ultrahigh vacuum in the SEM. This organic matrix may have created localized areas of reduced water activity due to organic−water interactions that assisted crystal growth.

3.2. Implications for CO_2 Sequestration. Modern (i.e., Holocene epoch) sedimentary magnesite-forming environments are rare, only forming under unique conditions such as those found in freshwater Mg-carbonate playas that are associated with ultramafic rocks[26,30] and highly evaporative coastal environments such as the Coorong saltwater lagoons in South Australia.[50,51] The scarcity of magnesite-forming systems is in stark contrast to the vast Ca-carbonate deposits on Earth, which contain roughly five million times more carbon in comparison to annual global greenhouse gas emissions,[1,3] despite magnesite (SI = 0.73) being more supersaturated in seawater than calcite (SI = 0.53). Presumably, the Earth's carbon cycle would be dramatically different if magnesite formed with the same ease as calcium carbonate—deposits of magnesite would be globally expansive and store massive amounts of Earth's carbon. With regard to stability, magnesite occurring in freshwater playas has formed over 100s to 1000s of years, suggesting a level of stability required for long-term storage of CO_2.[1] As is the case for dolomite, the estimated precipitation rate for magnesite at Earth's surface conditions[11] may be sufficient to explain its occurrence in the geologic record, yet is exceedingly too slow to garner interest as a pathway for permanent storage of anthropogenic CO_2. Using high-density carboxylated surfaces to accelerate magnesite formation at ambient temperature could lend itself to securely storing CO_2.

One approach to ex situ mineral carbonation involves the reaction of ultramafic rocks with CO_2 at high temperatures and pressures to form magnesite and silica.[3] Although magnesite formation occurs relatively rapidly at high temperature and pressure, carbonation rates may still be limited by magnesite precipitation.[29] Furthermore, the costs for pretreatment, energy use, and chemical inputs for ex situ mineral carbonation at high temperature (~$50−300/t CO_2) greatly exceed current carbon prices (e.g., California Carbon Allowance ≈ $13 US/t), severely limiting the application of these technologies.[3] Carbonation at ambient temperature and pressure generally requires more favorable chemical conditions in terms of pH and Mg and dissolved inorganic carbon concentrations for the precipitation of metastable hydrated Mg-carbonate minerals than those required to reach magnesite saturation. For instance, nesquehonite precipitates at near equilibrium conditions (e.g., SI ≈ 0) during aqueous carbonation of brucite $[Mg(OH)_2]$, whereas magnesite remains highly supersaturated (e.g., SI ≈ 2.7).[52] In our experiments, precipitation occurred in solutions only slightly supersaturated with respect to magnesite and without additional energy input. Moreover, microscopy of the final solids indicates that the carboxylated spheres were not consumed during reaction, indicating that further reaction is possible.

An alternative to silicate and hydroxide mineral feedstocks is to use evaporite deposits, waste brines, produced waters from oil extraction, and a virtually unlimited supply of seawater as feedstock for carbonate precipitation, thereby eliminating the need for mineral dissolution.[1] The abundance of readily available cation sources provides large CO_2 sequestration capacity.[1] For instance, the oil industry generates an estimated 8 Gt/yr of produced water, and 10 Gt/yr of reject brines with

DOI: 10.1021/acs.cgd.7b00311
Cryst. Growth Des. 2017, 17, 5652−5659

Mg concentrations ranging from 30 to 60 g/L and 0.5 to 20 g/L, respectively.[53] In comparison to seawater,[54] the compositions of these waters are highly variable.[55] Seawater is supersaturated with respect to magnesite (SI ≈ 0.7), whereas hydrated Mg-carbonate minerals such as hydromagnesite are undersaturated (SI ≈ −5.7), and therefore offer no carbon sequestration capacity. On the other hand, equilibrium precipitation of magnesite from seawater would sequester 2.0 g CO_2/L if pH were maintained and seawater kept at equilibrium with atmospheric CO_2. Upscaling the processes of magnesite precipitation demonstrated in this study could prove to be advantageous for ex situ carbonation strategies. The use of organic ligands for enhancing silicate dissolution for mineral carbonation has been shown to have an inhibitory effect on carbonate precipitation rates.[56] Researchers attribute this effect to the formation of surface complexes on the carbonate mineral or changing of the saturation state of the fluid.[56−61]

Geologic CO_2 sequestration involves injection of CO_2 into subsurface geologic formations including saline aquifers as well as mafic and ultramafic bodies.[62−65] Long-term (1000+ years) storage of CO_2 preferably relies on precipitation of carbonate minerals in the subsurface. Magnesite has been produced by reacting synthetic forsterite with wet $scCO_2$ at temperatures of 35 °C[16,47] and 50 °C,[66] conditions relevant to CO_2 injection into geologic reservoirs. Magnesite precipitation at 50 °C in $scCO_2$ (90 bar) correlates with the equilibrium constants for lignand−Mg^{2+} association reactions.[47] Miller et al.[47] suggest that ligand-promoted Mg^{2+} dehydration is likely enhanced in thin water films on mineral surfaces due to the highly ordered nature of this water that has dielectric constants that are much lower than bulk water phase, thereby enhancing ligand−H_2O exchange reactions. The presence of organic ligands able to partially dehydrate Mg^{2+} ions in the subsurface at $scCO_2$ injection sites may offer faster precipitation rates for securely storing CO_2. While upscaling our experimental systems remains a challenge, the potential for removing kinetic barriers for magnesite precipitation has implications for both ex situ and in situ carbonation processes at low temperature.

■ ASSOCIATED CONTENT

Supporting Information

The Supporting Information is available free of charge on the ACS Publications website at DOI: 10.1021/acs.cgd.7b00311.

Miller indices, lattice spacings and intensities for the aluminum standard, additional scanning electron micrographs, as well as X-ray and electron diffraction patterns of the aluminum standard and experimental precipitates (PDF)

■ AUTHOR INFORMATION

Corresponding Author

*E-mail: ianpower@trentu.ca

ORCID

Ian M. Power: 0000-0003-2102-9315

Notes

The authors declare no competing financial interest.

■ ACKNOWLEDGMENTS

Funding was provided by the Natural Sciences and Engineering Research Council of Canada (NSERC) Discovery grants to G.M.D. and M.R. From The University of British Columbia, we thank Gethin Owen at the Centre for High-Throughput Phenogenomics for assistance with scanning electron microscopy and Bradford Ross at the Bioimaging Facility for transmission electron microscopy. Special thanks to Todd Simpson at the Nanofabrication Laboratory, Western University, for thin section preparation.

■ REFERENCES

(1) Power, I. M.; Harrison, A. L.; Dipple, G. M.; Wilson, S. A.; Kelemen, P. B.; Hitch, M.; Southam, G. Carbon mineralization: From natural analogues to engineered systems. In *Geochemistry of Geologic CO_2 Sequestration*; DePaolo, D. J., Cole, D. R., Navrotsky, A., Bourg, I. C., Eds.; The Mineralogical Society of America: Chantilly, VA, 2013; Vol. *77*, pp 305−360.

(2) De Yoreo, J. J.; Waychunas, G. A.; Jun, Y. S.; Fernandez-Martinez, A. In Situ Investigations of Carbonate Nucleation on Mineral and Organic Surfaces. In *Geochemistry of Geologic CO_2 Sequestration*; DePaolo, D. J., Cole, D. R., Navrotsky, A., Bourg, I. C., Eds.; The Mineralogical Society of America: Chantilly, VA, 2013; Vol. *77*, pp 229−257.

(3) Sanna, A.; Uibu, M.; Caramanna, G.; Kuusik, R.; Maroto-Valer, M. M. A review of mineral carbonation technologies to sequester CO_2. *Chem. Soc. Rev.* **2014**, *43* (23), 8049−8080.

(4) Harrison, A. L.; Dipple, G. M.; Power, I. M.; Mayer, K. U. Influence of surface passivation and water content on mineral reactions in unsaturated porous media: Implications for brucite carbonation and CO_2 sequestration. *Geochim. Cosmochim. Acta* **2015**, *148*, 477−495.

(5) Wilson, S. A.; Harrison, A. L.; Dipple, G. M.; Power, I. M.; Barker, S. L. L.; Mayer, K. U.; Fallon, S. J.; Raudsepp, M.; Southam, G. Offsetting of CO_2 emissions by air capture in mine tailings at the Mount Keith Nickel Mine, Western Australia: Rates, controls and prospects for carbon neutral mining. *Int. J. Greenhouse Gas Control* **2014**, *25*, 121−140.

(6) McCutcheon, J.; Power, I. M.; Harrison, A. L.; Dipple, G. M.; Southam, G. A Greenhouse-Scale Photosynthetic Microbial Bioreactor for Carbon Sequestration in Magnesium Carbonate Minerals. *Environ. Sci. Technol.* **2014**, *48* (16), 9142−9151.

(7) Beinlich, A.; Austrheim, H. In situ sequestration of atmospheric CO_2 at low temperature and surface cracking of serpentinized peridotite in mine shafts. *Chem. Geol.* **2012**, *332*−*333*, 32−44.

(8) Wilson, S. A.; Barker, S. L. L.; Dipple, G. M.; Atudorei, V. Isotopic disequilibrium during uptake of atmospheric CO_2 into mine process waters: Implications for CO_2 sequestration. *Environ. Sci. Technol.* **2010**, *44*, 9522−9529.

(9) Montes-Hernandez, G.; Renard, F. Time-resolved in situ raman spectroscopy of the nucleation and growth of siderite, magnesite, and calcite and their precursors. *Cryst. Growth Des.* **2016**, *16* (12), 7218−7230.

(10) Königsberger, E.; Königsberger, L.; Gamsjager, H. Low-temperature thermodynamic model for the system Na_2CO_3-$MgCO_3$-$CaCO_3$-H_2O. *Geochim. Cosmochim. Acta* **1999**, *63*, 3105−3119.

(11) Saldi, G. D.; Jordan, G.; Schott, J.; Oelkers, E. H. Magnesite growth rates as a function of temperature and saturation state. *Geochim. Cosmochim. Acta* **2009**, *73* (19), 5646−5657.

(12) Schott, J.; Pokrovsky, O. S.; Oelkers, E. H. The Link Between Mineral Dissolution/Precipitation Kinetics and Solution Chemistry. In *Thermodynamics and Kinetics of Water-Rock Interaction*; Oelkers, E. H., Schott, J., Eds.; The Mineralogical Society of America: Chantilly, VA, 2009; Vol. *70*, pp 207−258.

(13) Gregg, J. M.; Bish, D. L.; Kaczmarek, S. E.; Machel, H. G. Mineralogy, nucleation and growth of dolomite in the laboratory and sedimentary environment: A review. *Sedimentology* **2015**, *62* (6), 1749−1769.

(14) Qafoku, O.; Dixon, D. A.; Rosso, K. M.; Schaef, H. T.; Bowden, M. E.; Arey, B. W.; Felmy, A. R. Dynamics of Magnesite Formation at Low Temperature and High pCO_2 in Aqueous Solution. *Environ. Sci. Technol.* **2015**, *49* (17), 10736−10744.

DOI: 10.1021/acs.cgd.7b00311
Cryst. Growth Des. 2017, 17, 5652−5659

(15) Qafoku, O.; Hu, J.; Hess, N. J.; Hu, M. Y.; Ilton, E. S.; Feng, J.; Arey, B. W.; Felmy, A. R. Formation of submicron magnesite during reaction of natural forsterite in H_2O-saturated supercritical CO_2. *Geochim. Cosmochim. Acta* **2014**, *134*, 197−209.
(16) Felmy, A. R.; Qafoku, O.; Arey, B. W.; Hu, J. Z.; Hu, M.; Schaef, H. T.; Ilton, E. S.; Hess, N. J.; Pearce, C. I.; Feng, J.; Rosso, K. M. Reaction of water-saturated supercritical CO_2 with forsterite: Evidence for magnesite formation at low temperatures. *Geochim. Cosmochim. Acta* **2012**, *91*, 271−282.
(17) Felmy, A. R.; Qafoku, O.; Arey, B. W.; Kovarik, L.; Liu, J.; Perea, D.; Ilton, E. S. Enhancing magnesite formation at low temperature and high CO_2 pressure: The impact of seed crystals and minor components. *Chem. Geol.* **2015**, *395*, 119−125.
(18) Hänchen, M.; Prigiobbe, V.; Baciocchi, R.; Mazzotti, M. Precipitation in the Mg-carbonate system - effects of temperature and CO_2 pressure. *Chem. Eng. Sci.* **2008**, *63* (4), 1012−1028.
(19) Land, L. S. Failure to precipitate dolomite at 25 °C from dilute solution despite 1000-fold oversaturation after 32 years. *Aquat. Geochem.* **1998**, *4*, 361−368.
(20) Vasconcelos, C.; McKenzie, J. A.; Bernasconi, S.; Grujic, D.; Tiens, A. J. Microbial mediation as a possible mechanism for natural dolomite formation at low temperatures. *Nature* **1995**, *377* (6546), 220−222.
(21) Kenward, P. A.; Fowle, D. A.; Goldstein, R. H.; Ueshima, M.; Gonzalez, L. A.; Roberts, J. A. Ordered low-temperature dolomite mediated by carboxyl-group density of microbial cell walls. *AAPG Bull.* **2013**, *97* (11), 2113−2125.
(22) Roberts, J. A.; Kenward, P. A.; Fowle, D. A.; Goldstein, R. H.; Gonzalez, L. A.; Moore, D. S. Surface chemistry allows for abiotic precipitation of dolomite at low temperature. *Proc. Natl. Acad. Sci. U. S. A.* **2013**, *110* (36), 14540−14545.
(23) Zhang, F. F.; Xu, H. F.; Konishi, H.; Shelobolina, E. S.; Roden, E. E. Polysaccharide-catalyzed nucleation and growth of disordered dolomite: A potential precursor of sedimentary dolomite. *Am. Mineral.* **2012**, *97* (4), 556−567.
(24) Parkhurst, D. L.; Appelo, C. A. J. Description of Input and Examples for PHREEQC Version 3—A Computer Program for Speciation, Batch-Reaction, One-Dimensional Transport, and Inverse Geochemical Calculations. In *U.S. Geological Survey Techniques and Methods*; U.S. Department of the Interior/U.S. Geological Survey: Washington, DC, **2013**; Chapter A43, Book 6, p 497.
(25) Bruker AXS. *DIFFRACplus EVA 14, Release 2008*; Karlsruhe, Germany, 2008.
(26) Power, I. M.; Wilson, S. A.; Harrison, A. L.; Dipple, G. M.; McCutcheon, J.; Southam, G.; Kenward, P. A. A depositional model for hydromagnesite−magnesite playas near Atlin, British Columbia, Canada. *Sedimentology* **2014**, *61*, 1701−1733.
(27) Falk, E. S.; Kelemen, P. B. Geochemistry and petrology of listvenite in the Samail ophiolite, Sultanate of Oman: Complete carbonation of peridotite during ophiolite emplacement. *Geochim. Cosmochim. Acta* **2015**, *160*, 70−90.
(28) Swanson, E. J.; Fricker, K. J.; Sun, M.; Park, A. H. A. Directed precipitation of hydrated and anhydrous magnesium carbonates for carbon storage. *Phys. Chem. Chem. Phys.* **2014**, *16* (42), 23440−23450.
(29) Saldi, G. D.; Schott, J.; Pokrovsky, O. S.; Gautier, Q.; Oelkers, E. H. An experimental study of magnesite precipitation rates at neutral to alkaline conditions and 100−200 degrees C as a function of pH, aqueous solution composition and chemical affinity. *Geochim. Cosmochim. Acta* **2012**, *83*, 93−109.
(30) Power, I. M.; Wilson, S. A.; Thom, J. M.; Dipple, G. M.; Gabites, J. E.; Southam, G. The hydromagnesite playas of Atlin, British Columbia, Canada: A biogeochemical model for CO_2 sequestration. *Chem. Geol.* **2009**, *260* (3−4), 286−300.
(31) Power, I. M.; Wilson, S. A.; Thom, J. M.; Dipple, G. M.; Southam, G. Biologically induced mineralization of dypingite by cyanobacteria from an alkaline wetland near Atlin, British Columbia, Canada. *Geochem. Trans.* **2007**, *8*, 13.
(32) Power, I. M.; Harrison, A. L.; Dipple, G. M. Accelerating Mineral Carbonation Using Carbonic Anhydrase. *Environ. Sci. Technol.* **2016**, *50* (5), 2610−2618.
(33) Harrison, A. L.; Dipple, G. M.; Power, I. M.; Mayer, K. U. The impact of evolving mineral-water-gas interfacial areas on mineral-fluid reaction rates in unsaturated porous media. *Chem. Geol.* **2016**, *421*, 65−80.
(34) Ming, D. W.; Franklin, W. T. Synthesis and characterization of lansfordite and nesquehonite. *Soil Science Society of America Journal* **1985**, *49* (5), 1303−1308.
(35) Wilson, S. A.; Dipple, G. M.; Power, I. M.; Barker, S. L. L.; Fallon, S. J.; Southam, G. Subarctic Weathering of Mineral Wastes Provides a Sink for Atmospheric CO_2. *Environ. Sci. Technol.* **2011**, *45* (18), 7727−7736.
(36) Di Lorenzo, F.; Rodríguez-Galán, R. M.; Prieto, M. Kinetics of the solvent-mediated transformation of hydromagnesite into magnesite at different temperatures. *Mineral. Mag.* **2014**, *78* (6), 1363−1372.
(37) Jiao, D.; King, C.; Grossfield, A.; Darden, T. A.; Ren, P. Y. Simulation of Ca^{2+} and Mg^{2+} solvation using polarizable atomic multipole potential. *J. Phys. Chem. B* **2006**, *110* (37), 18553−18559.
(38) Kluge, S.; Weston, J. Can a hydroxide ligand trigger a change in the coordination number of magnesium ions in biological systems. *Biochemistry* **2005**, *44*, 4877−4885.
(39) Di Tommaso, D.; de Leeuw, N. H. Structure and dynamics of the hydrated magnesium ion and of the solvated magnesium carbonates: insights from first principles simulations. *Phys. Chem. Chem. Phys.* **2010**, *12* (4), 894−901.
(40) Markham, G. D.; Glusker, J. P.; Bock, C. W. The arrangement of first- and second-sphere water molecules in divalent magnesium complexes: Results from molecular orbital and density functional theory and from structural crystallography. *J. Phys. Chem. B* **2002**, *106* (19), 5118−5134.
(41) Bock, C. W.; Kaufman, A.; Glusker, J. P. Coordination of water to magnesium cations. *Inorg. Chem.* **1994**, *33* (3), 419−427.
(42) Dudev, T.; Cowan, J. A.; Lim, C. Competitive binding in magnesium coordination chemistry: Water versus ligands of biological interest. *J. Am. Chem. Soc.* **1999**, *121*, 7665−7673.
(43) Wang, D.; Wallace, A. F.; De Yoreo, J. J.; Dove, P. M. Carboxylated molecules regulate magnesium content of amorphous calcium carbonates during calcification. *Proc. Natl. Acad. Sci. U. S. A.* **2009**, *106* (51), 21511−21516.
(44) Schultze-Lam, S.; Fortin, D.; Davis, B. S.; Beveridge, T. J. Mineralization of bacterial surfaces. *Chem. Geol.* **1996**, *132* (1−4), 171−181.
(45) Sikiric, M. D.; Fueredi-Milhofer, H. The influence of surface active molecules on the crystallization of biominerals in solution. *Adv. Colloid Interface Sci.* **2006**, *128−130*, 135−158.
(46) Sanz-Montero, M. E.; Rodríguez-Aranda, J. P. Magnesite formation by microbial activity: Evidence from a Miocene hypersaline lake. *Sediment. Geol.* **2012**, *263−264*, 6−15.
(47) Miller, Q. R. S.; Kaszuba, J. P.; Schaef, H. T.; Bowden, M. E.; McGrail, B. P. Impacts of Organic Ligands on Forsterite Reactivity in Supercritical CO_2 Fluids. *Environ. Sci. Technol.* **2015**, *49* (7), 4724−4734.
(48) de Leeuw, N. H.; Parker, S. C. Surface-water interactions in the dolomite problem. *Phys. Chem. Chem. Phys.* **2001**, *3* (15), 3217−3221.
(49) Xu, J.; Yan, C.; Zhang, F. F.; Konishi, H.; Xu, H. F.; Teng, H. H. Testing the cation-hydration effect on the crystallization of Ca-Mg-CO_3 systems. *Proc. Natl. Acad. Sci. U. S. A.* **2013**, *110* (44), 17750−17755.
(50) Melezhik, V. A.; Fallick, A. E.; Medvedev, P. V.; Makarikhin, V. V. Palaeoproterozoic magnesite: lithological and isotopic evidence for playa/sabkha environments. *Sedimentology* **2001**, *48* (2), 379−397.
(51) Wright, D. T.; Wacey, D. Precipitation of dolomite using sulphate-reducing bacteria from the Coorong Region, South Australia: significance and implications. *Sedimentology* **2005**, *52*, 987−1008.
(52) Harrison, A. L.; Power, I. M.; Dipple, G. M. Accelerated Carbonation of Brucite in Mine Tailings for Carbon Sequestration. *Environ. Sci. Technol.* **2013**, *47* (1), 126−134.

DOI: 10.1021/acs.cgd.7b00311
Cryst. Growth Des. 2017, 17, 5652−5659

(53) Mignardi, S.; De Vito, C.; Ferrini, V.; Martin, R. F. The efficiency of CO_2 sequestration via carbonate mineralization with simulated wastewaters of high salinity. *J. Hazard. Mater.* **2011**, *191* (1−3), 49−55.
(54) Nordstrom, D. K.; Plummer, L. N.; Wigley, T. M. L.; Wolery, T. J.; Ball, J. W.; Jenne, E. A.; Bassett, R. L.; Crerar, D. A.; Florence, T. M.; Fritz, B.; Hoffman, M.; Holdren, G. R., Jr.; Lafon, G. M.; Mattigod, S. V.; McDuff, R. E.; Morel, F.; Reddy, M. M.; Sposito, G.; Thrailkill, J. A comparison of computerized chemical models for equilibrium calculations in aqueous systems. In *Chemical Modeling in Aqueous Systems: Speciation, Sorption, Solubility, and Kinetics*; Jenne, E. A., Ed.; American Chemical Society: Washington, DC, 1979; pp 857−892.
(55) Blondes, M. S.; Gans, K. D.; Rowan, E. L.; Thordsen, J. J.; Reidy, M. E.; Engle, M. A.; Kharaka, Y. K.; Thomas, B. *U.S. Geological Survey National Produced Waters Geochemical Database v2.2*; U.S. Department of the Interior/U.S. Geological Survey: Washington, DC, 2017.
(56) Gautier, Q.; Berninger, U.-N.; Schott, J.; Jordan, G. Influence of organic ligands on magnesite growth: A hydrothermal atomic force microscopy study. *Geochim. Cosmochim. Acta* **2015**, *155*, 68−85.
(57) Bonfils, B.; Julcour-Lebigue, C.; Guyot, F.; Bodénan, F.; Chiquet, P.; Bourgeois, F. Comprehensive analysis of direct aqueous mineral carbonation using dissolution enhancing organic additives. *Int. J. Greenhouse Gas Control* **2012**, *9*, 334−346.
(58) Gautier, Q.; Bénézeth, P.; Schott, J. Magnesite growth inhibition by organic ligands: An experimental study at 100, 120 and 146 degrees °C. *Geochim. Cosmochim. Acta* **2016**, *181*, 101−125.
(59) Reddy, M. M.; Hoch, A. R. Calcite crystal growth rate inhibition by polycarboxylic acids. *J. Colloid Interface Sci.* **2001**, *235* (2), 365−370.
(60) Westin, K.; Rasmuson, A. C. Crystal growth of aragonite and calcite in presence of citric acid, DTPA, EDTA and pyromellitic acid. *J. Colloid Interface Sci.* **2005**, *282* (2), 359−369.
(61) Ganor, J.; Reznik, I. J.; Rosenberg, Y. O. Organics in Water-Rock Interactions. In *Thermodynamics and Kinetics of Water-Rock Interaction*; Oelkers, E. H., Schott, J., Eds.; The Mineralogical Society of America: Chantilly, VA, 2009; Vol. *70*, pp 259−369.
(62) Thom, J.; Dipple, G. M. Serpentine dissolution kinetics and rates of CO_2 sequestration. In *American Geophysical Union Fall Meeting Supplement*, San Francisco, CA, Dec 11−15, 2006; AGU: Washington, DC; 2006; Abstract V53D-1785.
(63) Power, I. M.; Wilson, S. A.; Dipple, G. M. Serpentinite carbonation for CO_2 sequestration. *Elements* **2013**, *9*, 115−121.
(64) Cipolli, F.; Gambardella, B.; Marini, L.; Ottonello, G.; Zuccolini, M. V. Geochemistry of high-pH waters from serpentinites of the Gruppo di Voltri (Genova, Italy) and reaction path modeling of CO_2 sequestration in serpentinite aquifers. *Appl. Geochem.* **2004**, *19* (5), 787−802.
(65) Matter, J. M.; Stute, M.; Snaebjörnsdottir, S. O.; Oelkers, E. H.; Gislason, S. R.; Aradottir, E. S.; Sigfusson, B.; Gunnarsson, I.; Sigurdardottir, H.; Gunnlaugsson, E.; Axelsson, G.; Alfredsson, H. A.; Wolff-Boenisch, D.; Mesfin, K.; Taya, D. F. D. l. R.; Hall, J.; Dideriksen, K.; Broecker, W. S. Rapid carbon mineralization for permanent disposal of anthropogenic carbon dioxide emissions. *Science* **2016**, *352* (6291), 1312−1314.
(66) Schaef, H. T.; McGrail, B. P.; Loring, J. L.; Bowden, M. E.; Arey, B. W.; Rosso, K. M. Forsterite [Mg_2SiO_4)] Carbonation in Wet Supercritical CO_2: An in Situ High-Pressure X-ray Diffraction Study. *Environ. Sci. Technol.* **2013**, *47* (1), 174−181.

DOI: 10.1021/acs.cgd.7b00311
Cryst. Growth Des. 2017, 17, 5652−5659